



Spatial variations of CO₂ fluxes in the Saguenay Fjord (Québec, Canada) and results of a water mixing model

Louise Delaigue¹, Helmuth Thomas² and Alfonso Mucci¹

¹GEOTOP and Department of Earth and Planetary Sciences, McGill University, 3450 University Street, Montreal, QC H3A 0E8, Canada

²Department of Oceanography, Dalhousie University, Halifax, Nova Scotia, Canada (now at Center for Materials and Coastal Research, Helmholtz-Zentrum Geesthacht, Germany)

Correspondence to: Louise Delaigue (louise.delaigue@mail.mcgill.ca)

Abstract. The Saguenay Fjord is a major tributary of the St. Lawrence Estuary and is strongly stratified. A 6-8 m wedge of brackish water typically overlies up to 270 m of seawater. Relative to the St. Lawrence River, the surface waters of the Saguenay Fjord are less alkaline and host higher dissolved organic carbon (DOC) concentrations. In view of the latter, surface waters of the fjord are expected to be a net source of CO₂ to the atmosphere, as they partly originate from the flushing of organic-rich soil porewaters. Nonetheless, the intrusion, at the surface, of brackish water from the upper estuary with the rising tide, as well as mixing of seawater, overflowing the sill from the lower estuary, modulate the CO₂ dynamics in the fjord. Using geochemical and isotopic tracers, in combination with an optimization multiparameter algorithm (OMP), we determined the relative contribution of known source-waters to the water column in the Saguenay Fjord, including waters that originate from the Lower St. Lawrence Estuary and replenish the fjord's deep basins. These results, when combined to a conservative mixing model and compared to field measurements, serve to identify the dominant factors, other than physical mixing, such as biological activity (photosynthesis, respiration) and gas exchange at the air-water interface, that impact the water properties (e.g., pH, pCO₂) of the fjord. Results indicate that the fjord's surface waters are a net source of CO₂ to the atmosphere during periods of high freshwater discharge (e.g., spring freshet) whereas they serve as a net sink of atmospheric CO₂ when their practical salinity exceeds ~ 5-10.

1 Introduction

Anthropogenic emissions of carbon dioxide (CO₂) have recently propelled atmospheric CO₂ concentrations above the 410 ppm mark, the highest concentration recorded in the past 800,000 years (Lüthi et al., 2008). The oceans, the largest CO₂ reservoir on Earth, have taken up ca. 30% of the anthropogenic CO₂ emitted to the atmosphere since the beginning of the industrial era (Brewer and Peltzer, 2009; Doney et al., 2009; Orr, 2011), mitigating the impact of this greenhouse gas on global warming. On the other hand, the uptake of CO₂ by the oceans has led to modifications of the seawater carbonate chemistry and a decline in the average surface ocean pH by ~0.1 units since pre-industrial times, a phenomenon dubbed ocean acidification (Caldeira, 2005). According to the Intergovernmental Panel on Climate Change (IPCC) "business as usual" emissions scenario IS92a and general circulation models, atmospheric CO₂ levels may reach 800 ppm by 2100, lowering the pH of the surface oceans by an additional 0.3-0.4 units, at a rate that is unprecedented in the geological record (Caldeira, 2005; Hönlisch et al.,



35 2012; Rhein et al., 2013). The growing concern about the impacts of anthropogenic CO₂ emissions on climate as
well as marine and terrestrial ecosystems calls for a meticulous quantification of organic and inorganic carbon
fluxes, especially in coastal environments, including fjords, a major but poorly quantified component of the global
carbon cycle and budget (Bauer et al., 2013). While much attention has recently focused on high latitude waters
40 (e.g., Arctic Ocean), coastal, seasonally ice-covered aquatic environments such as the Saguenay Fjord have
displayed comparable inter-annual and climatic sea-ice cover variabilities (Bourgault et al., 2012). Characteristics of
Arctic coastal ecosystems are found in the Saguenay Fjord, including the presence of many species of plankton, fish,
birds and marine mammals as well as important freshwater inputs and the presence of seasonal ice cover (Bourgault
et al., 2012).

This study presents 1) the relative contribution of known source waters to the water column in the fjord,
45 estimated from the solution of an optimization multiparameter algorithm (OMP) using geochemical and isotopic
tracers, and 2) results of a conservative mixing model, based on results of the OMP analysis and from which
theoretical surface-water pCO₂ values are derived and then compared to field measurements. The latter comparison
serves to identify the dominant factors, other than physical mixing (i.e. biological activity, gas exchange), that
impact the CO₂ fluxes at the air-sea interface throughout the fjord and modulate the trophic status of the fjord (i.e.
50 whether it is a source or a sink of CO₂ to the atmosphere).

2 Data and methods

2.1 Study site characteristics

Located in the subarctic region of Québec, eastern Canada, the Saguenay Fjord is up to 275 m deep, 110
km long and has an average width of 2 km, with a 1.1 km wide mouth where it connects to the head of the Lower St.
55 Lawrence Estuary (Fig. 1.a). The fjord's bathymetry includes three basins bound by three sills (Fig. 1.b). The first
one, at a depth of ~20 m, is located at its mouth near Tadoussac and controls the overall dynamics of the fjord. The
second is located 18 km further upstream and sits at a depth of 60 m, while the third one is found another 32 km
further upstream and rises to a depth of 115 m. The fjord's drainage basin is 78,000 km² and is part of the greater St.
Lawrence drainage basin (Smith and Walton, 1980), forming a hydrographic system, along with the Great Lakes, of
60 more than 1.36 million km².

Tributaries to the Saguenay Fjord include the Saguenay, Éternité and Sainte-Marguerite Rivers (Fig. 1.b).
The Saguenay River is the main outlet from the Saint-Jean Lake, and flows into the North Arm of the fjord near St.
Fulgence (Fig. 1.b) with a mean freshwater discharge of ~1200 m³ s⁻¹ (Bélanger, 2003). Two other local, minor
tributaries, the Rivière-à-Mars (95 km long, mean discharge ~8 m³ s⁻¹) and the Rivière des Ha! Ha! (35 km long,
65 mean discharge ~15 m³ s⁻¹) discharge into the Baie des Ha! Ha!, a distinct feature of the Saguenay Fjord. Finally, the
fjord receives denser marine waters from the St. Lawrence Estuary, filling the bottom of the three basins, as these
waters episodically overflow the entrance sill (Therriault and Lacroix, 1975; Stacey and Gratton, 2001; Bélanger,
2003; Belzile et al., 2016).



The overflow and the intrusion of marine waters from the St. Lawrence Estuary generate a sharp halocline, leading to a simplified two-layer stratification in the fjord (Fig 1.b). The tidally-modulated intrusion of marine waters from the St. Lawrence Estuary into the Saguenay Fjord, as well as the outflow of the fjord into the estuary, have a major influence on the water column stratification and circulation in the Saguenay Fjord and at its mouth (Belzile et al., 2016; Mucci et al., 2018). In other words, the properties of the uppermost 100 m of the water column in the adjacent estuary are critical in determining the water stratification in the Saguenay Fjord, since salinity and temperature control the density of waters that spill over the sill and fill the fjord's deep basins (Belzile et al., 2016). During most of the ice-free season, the St. Lawrence Estuary is characterized by three distinct layers: (1) a relatively warm and salty bottom layer (LSLE, $4^{\circ}\text{C} < T_{\text{max}} < 6^{\circ}\text{C}$, $34 < S_{\text{p}} < 34.6$) that originates from mixing, on the continental shelf, of northwestern Atlantic and Labrador Current waters, (2) a cold intermediate layer (CIL, 150 m deep; $-1^{\circ}\text{C} < T_{\text{max}} < 2^{\circ}\text{C}$, $31.5 < S_{\text{p}} < 33$) that forms in the Gulf of St. Lawrence in the winter and flows landward, and (3) a warm brackish surface layer (25-50 m deep, $25 < S_{\text{p}} < 32$) that results from the mixture of freshwater from various tributaries (mostly the St. Lawrence and Saguenay Rivers, but also north shore rivers such as the Betsiamites, Romaine and Manicouagan) and seawater and flows seaward to ultimately form the Gaspé Current (Dickie and Trites, 1983; El-Sabh and Silverberg, 1990; Gilbert and Pettigrew, 1997). Seasonal variations greatly affect the properties of the surface layer which merges with the intermediate layer during winter, as temperature and salinity change with atmospheric and buoyancy forcing and the contribution from tributaries decreases during winter months (Galbraith, 2006).

Likewise, the Saguenay Fjord is characterized by a strongly stratified water column that includes at least two water masses: (1) a warm, shallow layer, the Saguenay Shallow Water (SSW; $0^{\circ}\text{C} < T < 16.8^{\circ}\text{C}$, $0.2 < S_{\text{p}} < 26.9$), that lies above (2) the Saguenay Deep Water (SDW; $0.9^{\circ}\text{C} < T < 4.0^{\circ}\text{C}$, $27.3 < S_{\text{p}} < 29.8$). The SDW most likely forms from a mixture of surface fjord water, St. Lawrence River waters and the St. Lawrence Estuary Cold Intermediate Layer (CIL), when the latter spills over the entrance sill at the mouth of the fjord (Bourgault et al., 2012; Belzile et al., 2016). Nonetheless, our study shows that, because the Saguenay Fjord is a relatively deep fjord with multiple sills, the vertical structure of the water column is far more complex than described above.

2.2 Water-column sampling

The data presented in this paper were gathered on five cruises, between the years 2014 and 2018 aboard the R/V Coriolis II, in late spring (May 2016 and May 2018) and early summer (June 2017), as well as early and late fall (September 2014 and November 2017). Sampling of the water column was carried out with a rosette system along the central axis of the Saguenay Fjord, between St. Fulgence and the mouth of the fjord, including the Baie des Ha! Ha!. Stations in the St. Lawrence Estuary, near the mouth of the fjord, were also sampled. The sampling locations are identified in Fig. (1.a). The surface water of the Saguenay River was sampled, with a rope and bucket in 2013 and 2017, from the Dubuc Bridge that joins Chicoutimi and Chicoutimi-Nord, to determine the chemical characteristics of the freshwater Saguenay River end-member.

The rosette system (12 x 12-L Niskin bottles) was equipped with a Seabird 911Plus conductivity-temperature-depth (CTD) probe, a Seabird® SEB-43 oxygen probe, a WETLabs® C-Star transmissometer and a



105 Seapoint® fluorometer. The Niskin bottles were closed at discrete depths as the rosette was raised from the bottom,
typically at the surface (2-3 m), 25 m, 50 m, 75 m, 100 m, and at 50 m intervals to the bottom (or within 10 m of the
bottom). Samples were taken directly from the bottles for dissolved oxygen (DO), $\text{pH}_{(\text{NBS})}$ and/or $\text{pH}_{(\text{total})}$, total
alkalinity (TA), dissolved inorganic carbon (DIC), dissolved silicate (DSi), practical salinity (S_P), and the stable
oxygen isotopic composition of the water ($\delta^{18}\text{O}_{\text{water}}$). Water samples destined for pH measurements were transferred
110 to 125 mL plastic bottles without headspace whereas TA and TA/DIC samples were stored in, respectively, 250 mL
and 500 mL glass bottles. TA and TA/DIC samples were poisoned with a few crystals of mercuric chloride (HgCl_2)
and bottles were sealed using a ground-glass stopper and Apiezon® Type-M high-vacuum grease. $\delta^{18}\text{O}_{\text{water}}$ and S_P
samples were stored in 13 mL plastic screw-cap test tubes.

Direct measurements of surface water (~ 2 m) pCO_2 were carried out using a CO_2 -Pro CV (Pro-Oceanus,
115 Bridgewater, NS) probe in May 2018. The CO_2 -Pro CV probe operates through rapid diffusion of gases through a
supported semi-permeable membrane to a thermostated cell in which the CO_2 mole fraction is quantified by a non-
dispersive infrared detector (NDIR) that was factory calibrated using standard trace gas mixtures. The instrument
was operated in continuous mode, with measurements taken nearly every 7 seconds. Stable pCO_2 values were
achieved after a 15-minute equilibration period and averaged over the next 20 minutes. Relative standard deviations
120 over this period were typically on the order of 0.2 to 6% but were on the order of 0.1% in a stable water mass at 220
m depth, implying that deviations recorded at the surface likely reflected natural variations over the period of
sampling as the ship drifted with the current. The manufacturer claims a 1% accuracy, but the performance of the
instrument may be even better (Hunt et al., 2017).

Total freshwater discharge data of the Saguenay River were provided by Rio Tinto Alcan from their bank
125 stabilization programme. Data for the relevant sampling days in September 2014, May 2016, June 2017, November
2017 and May 2018 were taken from the Shipshaw and Chute-à-Caron monitoring stations.

2.3 Analytical procedures

T and S_P were determined in-situ using the CTD probe. The conductivity probe was calibrated by the
manufacturer over the winter prior to the cruises. In addition, the S_P of surface waters was determined by
130 potentiometric argentometric titration at McGill University and calibration of the AgNO_3 titrant with IAPSO
standard seawater. The reproducibility of these measurements is typically better than $\pm 0.5\%$.

pH_T was determined spectrophotometrically on board, on the total hydrogen ion concentration scale for
saline waters ($S_P > 5$), using phenol red and purified m-cresol purple as indicators and a Hewlett-Packard UV-visible
diode array spectrophotometer (HP-8453A) with a 5-cm quartz cell, after thermal equilibration of the sample in a
135 constant temperature bath at $25^\circ\text{C} \pm 0.1$. The salinity-dependence of the dissociation constants and molar
absorptivities of the indicators were taken from Robert-Baldo et al. (1985) for phenol red and from Clayton and
Byrne (1993) for m-cresol purple. The salinity-dependence of the phenol red indicator dissociation constant and
molar absorptivities was extended (from $S_P = 5$ to 35; Bellis, 2002) to encompass the range of salinities encountered
in this study, but computed pH_T values from the revised fit were not significantly different from those obtained with
140 the relationship provided by Robert-Baldo et al. (1985). Results computed from these parameters yielded results that



were more similar to each other as well as to potentiometric glass electrode measurements than the revised equation for the purified m-cresol purple provided by Douglas and Byrne (2017). The pH of low-salinity waters ($S_p < 5$) was determined potentiometrically on board at 25°C, on the NIST (formerly NBS) scale (pH_{NIST}), using a Radiometer Analytical® (GK2401C) combination glass electrode connected to a Radiometer Analytical® pH/millivoltmeter (PHM84). A calibration of the electrode was completed prior to and after each measurement, using three NIST-traceable buffer solutions: pH-4.00, pH-7.00 and pH-10.00, at 25°C. The Nernstian slope was then obtained from the least-squares fit of the electrode response to the NIST buffer values. For waters with S_p comprised between 5 and 35, pH_{NBS} was converted to pH_T according to the electrode response to TRIS buffer solutions prepared at $S_p = 5, 15, 25$ and 35 and for which the pH_T was assigned at 25°C (Millero, 1986). Reproducibility of pH measurements based on replicate analyses of the same sample or at least two of the three methods used was typically better than ± 0.005 . Dissolved oxygen (DO) concentrations were determined on board by Winkler titration on distinct water samples recovered directly from the Niskin bottles, following the method described by Grasshoff et al. (1999). The relative standard deviation, based on replicate analyses of samples recovered from the same Niskin bottle, was 0.5 %. These measurements served to calibrate the SBE-43 oxygen probe mounted on the rosette sampler.

The stable oxygen isotopic composition of the water samples ($\delta^{18}\text{O}_{\text{water}}$) was determined using the CO_2 equilibration method of Epstein and Mayeda (1953). Aliquots (200 μL) of the water samples and three laboratory internal reference waters were transferred into 3 mL vials stoppered with a septum cap. The vials were then placed in a heated rack maintained at 40°C. Commercially available CO_2 gas was introduced in all the vials using a Micromass AquaPrep and allowed to equilibrate for 7 hours. The headspace CO_2 was then sampled by the Micromass AquaPrep, dried on a -80°C water trap, and analyzed on a Micromass Isoprime universal triple collector isotope ratio mass spectrometer in dual inlet mode at the GEOTOP-UQAM Stable Isotope Laboratory. Data were normalized against the three internal reference waters, themselves calibrated against Vienna Standard Mean Ocean Water (V-SMOW) and Vienna Standard Light Arctic Precipitation (V-SLAP). The results are reported on the δ -scale in ‰ relative to V-SMOW:

$$\delta^{18}\text{O} = \left(\frac{(^{18}\text{O}/^{16}\text{O})_{\text{sample}}}{(^{18}\text{O}/^{16}\text{O})_{\text{standard}}} - 1 \right) \times 1000 \quad (1)$$

Based on replicate analyses of the samples, the average standard deviation of the measurements was better than 0.05‰.

TA was measured using an automated Radiometer (TitraLab865®) potentiometric titrator and a Red Rod® combination pH electrode (pHC2001) at McGill University. The dilute HCl titrant was calibrated prior, during and after each titration session using certified reference materials (CRM) provided by Andrew Dickson (Scripps Institution of Oceanography). Raw titration data were processed with a proprietary algorithm designed for shallow end-point detection. Surface water samples from the Saguenay Fjord and the Upper St. Lawrence Estuary were also analyzed at Dalhousie University using a VINDTA 3C® (Versatile Instrument for the Determination of Titration



Alkalinity, by Marianda) following the method described in Dickson et al. (2007). A calibration of the instrument was performed against CRMs and the reproducibility of the measurements was better than 0.1%.

The DIC concentration of samples, recovered in 2016, 2017 and 2018 in the Saguenay Fjord and surface waters of the Upper and Lower St-Lawrence Estuary, were determined at Dalhousie University using the VINDTA 3C®. In 2014, DIC was determined on board using a SciTech Apollo DIC analyzer. Once thermally equilibrated at 25°C, 1-1.5 mL of the sample was acidified with 10% H₃PO₄ after being injected into the instrument's reactor. The evolved CO₂ was carried to a LI-COR infrared analyzer by a stream of pure nitrogen. A calibration curve was constructed using gravimetrically prepared Na₂CO₃ solutions, and the accuracy of the measurements was verified using a CRM. Reproducibility was typically on the order of 0.2%.

185 2.4 Calculations

2.4.1 Water mass distribution analysis

A combination of transport processes associated with ocean circulation and biogeochemical cycles generally controls the distribution of tracers in the ocean (Chester, 1990). Resolving the effects of mixing and biogeochemical cycling is imperative if one is to evaluate the movement of nutrients and tracers in a water body. An Optimum Multi-Parameter (OMP) analysis allows for the determination of the relative contributions of pre-defined source-water types (SWT), representing the parameter values of the unmixed water masses in one specific geographic location, by optimizing the hydrographic data gathered in a given system (Tomczak, 1981). The original OMP algorithm is a linear inverse model that assumes all hydrographic tracers are conservative. The algorithm has since been modified to handle non-conservative properties such as DIC and nutrients by taking into consideration the stoichiometry of microbial respiration and photosynthesis (Dinauer and Mucci, 2018; Karstensen and Tomczak, 1998).

OMP calculates the SWT fractions, x_i , for each data point by finding the best linear mixing combination defined by parameters such as T, S_p, $\delta^{18}\text{O}_{\text{water}}$, DO, TA, and DIC. The contributions from all SWT must add-up to 100% and cannot be negative. Assuming that four SWT (a, b, c, and d) are sufficient to characterize the water column structure, and six parameters (T, S, $\delta^{18}\text{O}_{\text{water}}$, DO, TA, and DIC) characterize each of these, the following set of linear equations is solved in the classical OMP analysis (MATLAB - version 1.2.0.0; Karstensen, 2013):

$$x_a T_a + x_b T_b + x_c T_c + x_d T_d = T_{obs} + R_T \quad (2.a)$$

$$x_a S_a + x_b S_b + x_c S_c + x_d S_d = S_{obs} + R_S \quad (2.b)$$

$$205 \quad x_a \delta^{18}O_a + x_b \delta^{18}O_b + x_c \delta^{18}O_c + x_d \delta^{18}O_d = \delta^{18}O_{obs} + R_{\delta^{18}O} \quad (2.c)$$

$$x_a DO_a + x_b DO_b + x_c DO_c + x_d DO_d = DO_{obs} + R_{DO} \quad (2.d)$$

$$x_a TA_a + x_b TA_b + x_c TA_c + x_d TA_d = TA_{obs} + R_{TA} \quad (2.e)$$

$$x_a DIC_a + x_b DIC_b + x_c DIC_c + x_d DIC_d = DIC_{obs} + R_{DIC} \quad (2.f)$$

$$x_a + x_b + x_c + x_d = 1 + R_{\Sigma} \quad (2.g)$$



210 where T_{obs} , S_{obs} , $\delta^{18}O_{obs}$, DO_{obs} , TA_{obs} , and DIC_{obs} are the observed values in any given parcel of water and R_s
are their associated fitting residuals. T_i , S_i , $\delta^{18}O_i$, DO_i , TA_i , and DIC_i ($i = a, \dots, d$) are the characteristic values of
each SWT (Lansard et al., 2012; Tomczak and Large, 1989; Mackas et al., 1987). Mass conservation is expressed in
Eq. (2.g).

To account for potential environmental variability, measurement inaccuracies, and allow for the
215 comparison of parameters with incommensurable units, a weighting procedure based on covariances between tracers
is applied. In this study, weights were assigned arbitrarily based on their conservative behaviors and variability
(Lansard et al., 2012). Conservative tracers (i.e. S_p , TA , $\delta^{18}O_{water}$) were appointed heavy weights, while non-
conservative tracers (i.e. T , DO , DIC) were given low weights according to their seasonal variability. For instance,
temperatures in the surface waters of the Saguenay River range from 3.1°C in the winter to 21°C in the summer.
220 Dissolved oxygen was also considered a non-conservative tracer as it is heavily reliant on temperature and salinity,
as well as biological activity. DIC was given an intermediate weight given that it is relatively conservative except in
the surface waters, where photosynthesis and air-sea gas exchange take place.

2.4.2 Water mass distribution analysis

A water mass is, by definition, a body of water having its origin in a particular source region (Tomczak,
225 1999). An OMP analysis requires the user to define the major water masses contributing to the structure of the water
column in the study area. In the context of biogeochemical cycles, a SWT should be defined where the water mass
enters the basin, upstream from the mixing region (Karstensen, 2013). Parameter values are preferably extrapolated
from hydrographic observations in the water mass formation region or can be found in the literature.

In this study, source-water type definitions were derived from property-property diagrams (See Appendix,
230 Fig. A) of an observational dataset relevant to the Saguenay Fjord: the Saguenay River (SWR), the St. Lawrence
Estuary summertime Cold Intermediate Layer (CIL), the Lower St. Lawrence Estuary bottom waters (LSLE) and the
St. Lawrence River (SLRW). Each definition was captured relative to the fjord, i.e. each source-water type is only
appropriate for the fjord and for the period of study. Definitions and weights are reported in Table 1.

2.4.3 CO₂ partial pressures

235 The CO₂ partial pressure in seawater ($pCO_{2(SW)}$) is defined as the pCO_2 in water-saturated air ($pCO_{2(air)}$) in
equilibrium with the water sample or the ratio of the CO₂ concentration in solution to the equilibrium concentration
at T , P and S_p , multiplied by the actual $pCO_{2(air)}$. As direct measurements of the surface mixed layer pCO_2 were not
available in September 2014, May 2016, June 2017 and November 2017, it was calculated ($pCO_{2(SW-calc)}$) using
CO2SYS (Excel v2.1; Pierrot et al., 2006) and the measured pH (total or NBS/NIST scale), DIC ($\mu mol \cdot kg^{-1}$), in-situ
240 temperature (°C), practical salinity (S_p) and pressure (dbar) as input parameters. When available, soluble reactive
phosphate (SRP) and dissolved silicate (DSi) concentrations were also included in the calculations, but their
inclusion did not affect the results significantly because their concentrations are relatively low in surface waters
(0.49 μM and 37.0 μM , respectively) and introduce an insignificant error. DIC rather than TA was used as an input
parameter to CO2SYS since the fjord surface waters are enriched in colored dissolved organic carbon (> 4 mg/L)



245 delivered by the Saguenay River, and are characterized by a negative organic alkalinity (positive organic acidity)
(see below). The carbonic acid dissociation constants (K^*_1 and K^*_2) of Cai and Wang (1998) were used for the
calculations, as the latter were found to be more suitable for the low-salinity conditions encountered in estuarine
environments such as the Saguenay Fjord ($S_p < 20$) (Dinauer and Mucci, 2017). $pCO_{2(SW-calc)}$ values were computed
for the surface mixed layer located above the sharp pycnocline (~10 m) where most physical and chemical
250 properties are directly impacted by biological activity (photosynthesis and respiration) as well as heat and gas
exchange across the air-sea interface (Table 2). Direct measurements of pCO_2 ($pCO_{2(SW-meas)}$) were acquired in May
2018, and $pCO_{2(SW-calc)}$ were also calculated from pH and DIC for this sampling month for comparison purposes,
following the aforementioned procedure.

2.4.4 CO₂ flux across the air-sea interface

255 The difference between the air and sea-surface pCO_2 values ($\Delta pCO_2 = pCO_{2(SW)} - pCO_{2(air)}$) determines the
direction of gas exchange and whether the surface mixed layer of a body of water is a source or a sink of CO₂ for the
atmosphere. The air-sea CO₂ gas exchange, or CO₂ flux, can be estimated at each station using the following
relationship:

$$260 \quad FCO_2 = k \cdot K_0 \cdot (\Delta pCO_2) \quad (3.a)$$

where F is the flux of CO₂ across the air-sea interface in $mmol \cdot m^{-2} \cdot d^{-1}$, k is the gas transfer velocity of CO₂ in $cm \cdot h^{-1}$
(Wanninkhof, 1992), K_0 is the solubility of CO₂ in $mol \cdot kg^{-1} \cdot atm^{-1}$ at the in-situ temperature and salinity of the
surface waters (Weiss, 1974), and ΔpCO_2 is the difference between the air and sea-surface pCO_2 values in μatm .
265 Whereas, formally, Fick's first law of diffusion should be written as $F = -D \delta c / \delta x$, as commonly expressed by
Eq. (3.a), positive values of F indicate the release of CO₂ to the atmosphere by surface waters, whereas negative
values imply that surface waters serve as a sink of atmospheric CO₂. The flux of CO₂ was computed for each
sampling month, using the $pCO_{2(air)}$ for each sampling date (395 μatm for September 2014, and 407 μatm for May
2016, 408 μatm for June and November 2017, and 411 μatm for May 2018 – see below for details).

270 The gas transfer velocity of CO₂ was calculated using the revised relationship of Wanninkhof (2014):

$$k = 0.215u^2 (Sc/660)^{-1/2} \quad (3.b)$$

where u is the wind speed ($m \cdot s^{-1}$) and Sc is the Schmidt number (Wanninkhof, 2014). Wind speed was estimated
275 using the hourly station wind speed data from Environment Canada at the La Baie weather station, for each
sampling month. The Schmidt number is defined as the kinematic viscosity of water divided by the diffusion
coefficient of CO₂. Sc was corrected for the temperature dependence of CO₂ in freshwater ($S_p = 0$), assuming that k
is proportional to $Sc^{-1/2}$ (Wanninkhof, 1992). In the case of CO₂, the increase in $Sc^{-1/2}$ (and k) with increasing
temperature is compensated for by a decrease in solubility, therefore k was considered nearly temperature
280 independent (Wanninkhof, 1992). Sc was computed using:



$$Sc = A + Bt + Ct^2 + Dt^3 + Et^4 \quad (3.c)$$

where t is the temperature (degrees Celcius) and A, B, C, D and E are fitting coefficients for seawater ($S_P = 35$) and
285 freshwater ($S_P = 0$), for temperatures ranging from -2°C to 40°C (Wanninkhof, 2014). The uncertainty in Sc ranges
from 3 to 10% and is mainly due to the imprecision of diffusion coefficients (Wanninkhof, 2014). Estimates of k ,
calculated at each sampling point using the equation of Wanninkhof (2014), ranged from 0.36 to $3.38 \text{ cm}\cdot\text{h}^{-1}$ for the
fjord, compared to 1.6 to $4.5 \text{ cm}\cdot\text{h}^{-1}$ in the St. Lawrence Estuary (Dinauer and Mucci, 2017).

Atmospheric $p\text{CO}_2$ values ($p\text{CO}_{2(\text{air})}$) were computed using the daily averages of measured mole fractions
290 of CO_2 in dry air, obtained at the La Baie weather station and retrieved from the Climate Research Division at
Environment and Climate Change Canada. The mean $p\text{CO}_{2(\text{air})}$ was then calculated for each year using the following
equation:

$$p\text{CO}_{2(\text{air})} = x\text{CO}_2 \cdot (P_b - P_w) \quad (4)$$

295 where $x\text{CO}_2$ is the measured mole fraction of CO_2 in dry air in ppm, P_b is the barometric pressure at the sea surface
in atm, and P_w is the saturation water vapor pressure at in-situ temperature and salinity, in atm. P_b was obtained
using the conversion formula of Tim Brice and Todd Hall (from NOAA's National Weather Service), using the La
Baie weather station's elevation (152 m). P_w was calculated using the Rivière-à-Mars properties (i.e. closest body of
300 water to the weather station) and the P_w calculated from its relationship to T and S_P provided by Weiss and Price
(1980).

The area-averaged CO_2 flux ($F_{\text{area-avg}}$) was computed for the whole fjord, following the procedure described
by Jiang et al. (2008):

$$305 \quad F_{\text{area-avg}} = \frac{\sum F_i \times S_i}{\sum S_i} \quad (5)$$

where F_i is the average of all the fluxes within segment i , and S_i is the surface area of segment i . The fjord's surface
area ($\sim 290 \text{ km}^2$) was computed using a land mask in MATLAB.

2.4.5 Water Mixing Model

310 A two end-member mixing model was constructed based on the chemical properties of the freshwater delivered
to the fjord (Saguenay River) and marine bottom waters entering the fjord from the St. Lawrence Estuary (Fig. 2.a).
As shown in the results of the OMP analysis (Sect. 3.1), the LSLE and SLRW have a negligible influence on the
fjord's water structure, and thus were not included in the model. Given that the carbonate chemistries of the CIL and
LSLE waters are similar, the bottom waters were assumed to be well mixed and constitute a single end-member.
315 This is illustrated in Fig. (2), as the high S_P end-member alkalinity extends linearly beyond that of the CIL end-
member (Table 1). The measured surface TAs were strongly correlated to S_P ($R^2 = 0.99$) in the fjord waters.



Therefore, end-member properties were obtained by extrapolating the surface water (above the pycnocline) data to $S_P = 0$ and bottom-water data to the highest measured salinity (Fig. 2.a). The extrapolated $TA_{(meas)}$ (Fig 2.b; $154 \mu\text{mol}\cdot\text{kg}^{-1}$) is in good agreement with the average $TA_{(meas)}$ of samples taken directly from the Saguenay River in 2013 and 2017 ($157 \mu\text{mol}\cdot\text{kg}^{-1}$). The organic alkalinity of the fjord waters was estimated from the difference between the measured and calculated TA ($TA_{(calc)}$; Fig. 2.b). The latter was calculated using CO2SYS (Excel v2.1; Pierrot et al., 2006) and pH and DIC as input parameters. The end-member source waters were then mixed, assuming that $TA_{(calc)}$ and DIC behave conservatively. Hence, the salinity, total alkalinity ($TA_{(mix)}$) and dissolved inorganic carbon ($DIC_{(mix)}$) of the mixed solutions were calculated using the following equations:

325

$$S_{P(mix)} = \frac{m_1 S_{P1} + m_2 S_{P2}}{(m_1 + m_2)} \quad (6a)$$

$$TA_{(mix)} = \frac{m_1 TA_{(calc)-1} + m_2 TA_{(calc)-2}}{(m_1 + m_2)} \quad (6b)$$

$$DIC_{(mix)} = \frac{m_1 DIC_1 + m_2 DIC_2}{(m_1 + m_2)} \quad (6c)$$

330 where m_i are the mass contributions of each end-member to the mixture.

$p\text{CO}_{2(\text{SW-mix})}$ was then computed from $TA_{(mix)}$ and $DIC_{(mix)}$ for practical salinities ranging from 0 to 33, at four different temperatures (0°C , 5°C , 10°C and 15°C) using CO2SYS. Results of the model (Fig. 8) show that, at the lower and higher salinities, the $p\text{CO}_{2(\text{SW-mix})}$ is elevated, and the fjord serves as a net source of CO_2 to the atmosphere, but at intermediate salinities ($5 < S_P < 15$) or mixing ratios, the fjord may serve as a net sink of atmospheric CO_2 when surface water temperatures are close to freezing. The data from the various cruises are superimposed on the model results, after correction for the organic alkalinity.

335

2.4.6 Salinity normalization of DIC in surface waters

To quantitatively evaluate the impact of biological activity on the DIC budget in the surface waters of the fjord, DIC and $TA_{(calc)}$ were normalized to the average surface salinity of each sampling month ($S_P = 12.4$ for September 2014, $S_P = 2.58$ for May 2016, $S_P = 7.61$ for June 2017, $S_P = 10.9$ for November 2017 and $S_P = 5.9$ for May 2018) following the procedure of Friis et al. (2003):

340

$$\text{NDIC} = \frac{DIC^{meas} - DIC^{S=0}}{S^{meas}} \cdot S^{ref} + DIC^{S=0} \quad (7)$$

345 where DIC^{meas} is the measured DIC, $DIC^{S=0}$ is the DIC extrapolated to $S_P = 0$, S^{meas} is the measured practical salinity and S^{ref} is the average measured practical salinity per sampling month (Friis et al., 2003). The change in NDIC (i.e. ΔNDIC) along the fjord, relative to the waters at the head of the fjord, was then computed for each sampling month. These values reveal how DIC evolves along the fjord beyond what is expected based on conservative mixing.



350 2.4.7 Oxygen saturation and apparent oxygen utilization in the surface waters

To further account for the biological activity in the surface waters, the oxygen saturation index was calculated for each sampling month in the surface waters of the fjord using:

$$\% \text{ sat} = ([O_2]_{\text{meas}}/[O_2]_{\text{equil}}) \times 100 \quad (8)$$

355

where $[O_2]_{\text{meas}}$ is the dissolved oxygen concentration measured in the fjord waters, and $[O_2]_{\text{equil}}$ is the equilibrium dissolved oxygen concentration (or solubility) at in-situ conditions (i.e. temperature and salinity) for each sample.

The oxygen saturation index indicates if the system is autotrophic (i.e. production of oxygen, dominated by photosynthesis) or heterotrophic (consumption of oxygen, dominated by microbial respiration). The oxygen saturation remains a qualitative proxy as O_2 exchange at the air-sea interface is about 9 times faster than CO_2 exchange (Zeebe and Wolf-Gladrow, 2001). The apparent oxygen utilization (AOU) was also computed from the difference between $[O_2]_{\text{equil}}$ and $[O_2]_{\text{meas}}$.

3 Results and discussion

365 3.1 Water mass analysis

Relative contributions (mixing ratios, f) of the Saguenay River (SRW), Cold Intermediate Layer (CIL) from the St. Lawrence Estuary and Lower St. Lawrence Estuary (LSLE) bottom waters throughout the Saguenay Fjord's water column for the sampling month of June 2017 are shown in Fig. (3). As expected, the SRW and CIL are dominant contributors, with the SRW forming a brackish surface layer ($f = 1$ in surface waters), and the CIL replenishing the bottom waters of the fjord ($0.7 < f < 1$). According to the OMP analysis, the LSLE bottom waters have a small contribution to the fjord's bottom waters ($f = 0.2$), adding to the complexity of the water structure. Although somewhat unexpected, this can readily be explained by tidal upwelling, internal waves and intense turbulent mixing of the water column at the head of the Laurentian Channel (Gratton et al., 1988; Saucier and Chassé, 2000). The relative contribution of the LSLE bottom waters in the deep waters of the fjord is small and could only be detected because of the suite of geochemical and isotopic tracers used in the OMP analysis, especially the difference in the $\delta^{18}O_{\text{water}}$ signature of the CIL and LSLE waters. The contribution from the St. Lawrence River Water (SLRW) is negligible, as it intrudes slightly at the surface at the mouth of the fjord and is thus not shown here. Although the water column structure is similar throughout the year, seasonal variations do occur and will be addressed in a forthcoming paper.

380 3.2 Aqueous pCO_2 and CO_2 flux

Variations of the inorganic carbon chemistry in the Saguenay Fjord water column are described using field data acquired in September 2014, May 2016, June 2017, November 2017 and May 2018. The river drains the Canadian Shield and boreal forest soils, and carries organic acidity released from soil porewaters. The organic



alkalinity (acidity) accounted, on average, for 2.2% to 11.9% of the total alkalinity of the Saguenay River and varied
385 annually and seasonally ($-21 \mu\text{mol}\cdot\text{kg}^{-1}$ in September 2014, $-39 \mu\text{mol}\cdot\text{kg}^{-1}$ in May 2016, $-49 \mu\text{mol}\cdot\text{kg}^{-1}$ in June 2017,
 $-22 \mu\text{mol}\cdot\text{kg}^{-1}$ in November 2017 and $-18 \mu\text{mol}\cdot\text{kg}^{-1}$ in May 2018). It was inversely proportional to the salinity of
the surface waters of the fjord and became positive but a negligible fraction ($< 0.1\%$) of $\text{TA}_{(\text{corr})}$ at $S_P > 25$, like in
the St. Lawrence Estuary. Surface-water pCO_2 ($\text{pCO}_{2(\text{SW-calc})}$) values were higher at the head of the fjord (i.e. near
the Saguenay River mouth) and lower at the mouth of the fjord, although large variations ($315 \mu\text{atm}$ to $740 \mu\text{atm}$ –
390 average $503 \mu\text{atm}$) were observed on a seasonal and yearly basis (Table 2). Values of $\text{pCO}_{2(\text{SW})}$ were higher in May
2018 ($623 \mu\text{atm}$), June 2017 ($506 \mu\text{atm}$) and May 2016 ($563 \mu\text{atm}$) than in November 2017 ($418 \mu\text{atm}$) and
September 2014 ($406 \mu\text{atm}$). This can be explained by the larger freshwater discharge from the Saguenay River in
the spring (i.e. spring freshet, average of $1856 \pm 21 \text{ m}^3 \text{ s}^{-1}$ for spring periods of 1998 - 2018), compared to the fall
($1470 \pm 10 \text{ m}^3 \text{ s}^{-1}$ for fall periods of 1998 - 2018). As atmospheric $\text{pCO}_{2(\text{air})}$ varied marginally between September
395 2014 ($395 \mu\text{atm}$) and May 2018 ($411 \mu\text{atm}$), the fjord was generally a source of CO_2 to the atmosphere near its head
(i.e. surface pCO_2 values above atmospheric level), while the zone near its mouth was most often a sink (i.e. surface
 pCO_2 values below atmospheric level) (Fig. 4). An anomaly was observed in November 2017, with a high $\text{pCO}_{2(\text{SW-}$
 $\text{calc})}$ value ($> 550 \mu\text{atm}$) near the mouth of the fjord. Given the statistics of the box plot presented in Fig. (7), this
value appears to be erroneous.

400 Air-sea CO_2 fluxes within the fjord ranged from $-2.4 \text{ mmol}\cdot\text{m}^{-2}\cdot\text{d}^{-1}$ to $10.0 \text{ mmol}\cdot\text{m}^{-2}\cdot\text{d}^{-1}$ (Fig. 6). Near the
head of the fjord, fluxes were mostly positive, while values decreased when approaching its mouth. Overall, the total
area-averaged degassing flux of the fjord adds up to $2.14 \pm 0.43 \text{ mmol}\cdot\text{m}^{-2}\cdot\text{d}^{-1}$ (i.e. $0.78 \pm 0.16 \text{ mol}\cdot\text{m}^{-2}\cdot\text{yr}^{-1}$). In
comparison, the degassing flux in the adjacent St. Lawrence Estuary was estimated at between 0.36 and $0.74 \text{ mol}\cdot\text{m}^{-2}\cdot\text{yr}^{-1}$
405 during the late spring and early summer (Dinauer and Mucci, 2017). This discrepancy can be explained by the
low carbonate alkalinity (and buffer capacity) of the Saguenay River waters that flow through the Grenvillian
metamorphic and igneous rocks of the Canadian Shield (Piper et al., 1990), as with most rivers on the north shore of
the St. Lawrence Estuary (e.g., Betsiamites, Manicouagan, Romaine; Paul del Giorgio, pers. comm.), and the low
productivity of the fjord surface waters because of very limited light penetration due to their high chromotrophic
dissolved organic matter (CDOM) content (Tremblay and Gagné, 2009; Xie et al., 2012). In contrast, waters of the
410 St. Lawrence River have an elevated carbonate alkalinity ($\sim 1200 \mu\text{M}$), inherited from the Ottawa River that drains
through limestone deposits (Telmer and Veizer, 1999). Furthermore, the Estuary is host to multiple seasonal
phytoplankton blooms (Levasseur and Therriault, 1987; Zakardjian et al., 2000; Annane et al., 2015) that strongly
modulate its trophic status (Dinauer and Mucci, 2018).

The correlation between $\text{pCO}_{2(\text{SW-meas})}$ and $\text{pCO}_{2(\text{SW-calc})}$ is presented in Fig. (5). The average difference between
415 $\text{pCO}_{2(\text{SW-meas})}$ and $\text{pCO}_{2(\text{SW-calc})}$ is $48 \mu\text{atm}$, implying that calculations underestimate $\text{pCO}_{2(\text{SW})}$ values by
approximately 7% and thus contribute to the uncertainty associated with CO_2 fluxes. This discrepancy most likely
originates from uncertainties associated with the carbonic acid dissociation constants (K^*_1 and K^*_2) in low salinity
estuarine environments, particularly those affected by strong organic alkalinities or acidities such as the Saguenay
Fjord (Cai et al., 1998; Ko et al., 2016). This concurs with the results from Lueker et al. (2000) who showed that,
420 depending on the choice of K^*_1 and K^*_2 , computed $\text{pCO}_{2(\text{SW})}$ values from other carbonate system parameters (TA,



DIC, pH) can be up to 10% lower than those of direct measurements. Consequently, although the constants of Cai and Wang (1998) are the most suitable for this study, direct measurements of the $p\text{CO}_{2(\text{SW})}$ should preferentially be carried out whenever possible.

3.3 Water Mixing Model approach

425 As results of the OMP analysis reveal, LSLE and SLRW have a negligible influence on the water properties in the fjord, except for the latter near the mouth. Additionally, given the relatively small contribution of the LSLE deep waters and their similarity to the carbonate chemistry of the CIL, their influence is considered inconsequential on the properties of the mixture. Hence, a conservative mixing model was constructed based on the chemical properties of the two main source water masses in the fjord (i.e. SRW and the CIL mixture for bottom waters), and the
430 relationship between practical salinity and TA(corr)/DIC, respectively (Fig. 8). $p\text{CO}_{2(\text{SW-calc})}$ were normalized at each station to the average surface water temperature per sampling month (i.e., $T = 10.4^\circ\text{C}$ for September 2014, $T = 5.04^\circ\text{C}$ for May 2016, $T = 11.9^\circ\text{C}$ for June 2017, $T = 7.13^\circ\text{C}$ for November 2017 and $T = 5.08^\circ\text{C}$ for May 2018) to account for the effects of temperature on the CO_2 solubility in water, following the procedure described in Jiang et al. (2008). The temperature-normalized $p\text{CO}_{2(\text{SW-calc})}$ values, $p\text{CO}_{2(\text{SW-SST})}$, from the various cruises were
435 superimposed on the model results in Fig. (8).

Field measurements follow the trend displayed by the mixing model. The fjord appears to be a net source of CO_2 to the atmosphere during periods of high freshwater discharge (i.e. spring freshet) and a net sink at intermediate surface salinities ($5 < S_p < 15$). This is consistent with the weak buffer capacity of the freshwater. Given the short residence time of surface waters in the Saguenay Fjord (~ 1.5 days), the influence of gas exchange across the air-sea
440 interface is negligible on the DIC pool. Likewise, Dinauer and Mucci (2017) reported that the surface waters in the St. Lawrence Estuary near Tadoussac (at the mouth of the fjord) are highly supersaturated in CO_2 with respect to the atmosphere and only the highly productive waters of the Lower Estuary manage to draw down the surface $p\text{CO}_2$ to near atmospheric values. In other words, degassing of the metabolic CO_2 accumulated in the river and upper estuary is slow. Thus, changes in temperature-normalized $p\text{CO}_2$ primarily mostly reflect changes in DIC by mixing and
445 biological activity. Hence, discrepancies between results of the mixing model and field measurements can be ascribed to microbial respiration and photosynthesis.

In May 2016, the surface waters of the fjord were clearly supersaturated in oxygen (Fig. 9), implying that photosynthesis dominated over respiration. This would explain the rapid seaward (increasing S_p) decrease in $p\text{CO}_{2(\text{SW-SST})}$, faster than the mixing model predicts (Fig. 8), and the strong negative ΔNDIC (i.e. change in NDIC
450 relative to the saline waters at the head of the fjord) throughout the fjord (Fig. 10), as CO_2 (i.e. DIC) is taken up by photosynthesizing organisms - most likely diatoms (Chassé and Côté, 1991). In May 2018, surface waters were slightly undersaturated in oxygen, between 90% and 100% saturation, and ΔNDIC was positive over most of the fjord. Very similar trends were observed in June 2017, with near-saturation oxygen concentrations (between 95 and 101% saturation) and mostly positive ΔNDIC values throughout the transect. Thus, during these sampling periods,
455 biological activity was dominated by microbial respiration (Fig. 10), elucidating the minor deviation between the



$p\text{CO}_{2(\text{SW-SST})}$ and the model results (Fig. 8), especially near the head of the fjord. Additionally, it is interesting to note that ΔNDIC is chronically negative for all sampling months near the 45 km mark.

The difference between the May 2016 and May 2018 biological responses to the spring freshet can potentially be explained by the difference in total freshwater discharge from the Saguenay River to the fjord. The freshwater discharge in May 2018 was approximately 20% larger than in May 2016. Whereas the surface salinities recorded both years throughout most of the fjord were nearly identical ($S_p = 0.5\text{-}4$ in 2016, $S_p = 0.7\text{-}5$ in 2018), the greater delivery of soil porewater and associated CDOM in May 2018 may have inhibited local productivity due to light absorption by CDOM (Lavoie et al., 2007). Consistent with this interpretation is the fact that the $p\text{CO}_{2(\text{SW-SST})}$ at the head of the fjord (St. Fulgence) in May 2016 was slightly higher than in May 2018 but was drawn down much faster downstream (Fig. 8).

There does not appear to be a clear biological signal in the November 2017 data, as little variation is observed between the measured and modeled $p\text{CO}_2$. Furthermore, Fig. (10) indicates that neither respiration nor photosynthesis dominated during this period as the ΔNDIC varies between weakly positive and negative values. Likewise, the September 2014 data reveal little biological activity, although a slight dominance of respiration (i.e. positive ΔNDIC with a drop in $\%O_2$ saturation) can be observed near the mouth of the fjord (Fig. 10), hence explaining the slight deviation from the mixing model.

4 Summary and conclusions

Results of the OMP analysis reveal that SRW and CIL are the dominant source-water types to the fjord and determine the structure of its water column. Mixing of marine waters with SRW at the head of the fjord leads to the formation of a brackish surface layer (wedge) while the CIL replenishes the bottom waters of the fjord. The analysis further unveiled a small contribution of the LSLE bottom water to the bottom waters of the fjord, adding to the complexity of the water structure. The SLRW has a negligible influence on the water properties in the fjord, except near its mouth - sampling of the very turbulent waters directly over the fjord's first and shallowest sill would help refine the contribution of the SLRW to the fjord's surface waters.

The magnitude and sign of the $\Delta p\text{CO}_2$ across the air-water interface in the Saguenay Fjord, mostly determined by the $p\text{CO}_{2(\text{SW})}$ as $p\text{CO}_{2(\text{air})}$ varying only slightly over the sampling period, are mostly modulated by the freshwater discharge and the salinity of the surface waters. The surface waters of the fjord are a source of CO_2 to the atmosphere at high freshwater discharge, and a sink of CO_2 at intermediate surface salinities ($5 < S_p < 15$), especially at near-freezing temperatures. Direct measurements of $p\text{CO}_2$ acquired in May 2018 further validate this trend. Biological activity (photosynthesis and respiration) alters the surface-water $p\text{CO}_2$, with both photosynthesis and respiration impacting the waters depending on the sampling month. This conclusion is further supported by the oxygen saturations observed in the surface waters of the fjord, as well as the ΔNDIC trend. Given the short residence time of surface waters in the Saguenay Fjord (~ 1.5 days), the influence of gas exchange on spatial variations of the $\Delta p\text{CO}_2$ across the air-sea interface is negligible on the DIC pool. Overall, the fjord serves as a



490 source of CO₂ to the atmosphere during the ice-free season, with an average yearly outgassing flux of 0.78 ± 0.16
mol·m⁻²·yr⁻¹.

495

500

505

510

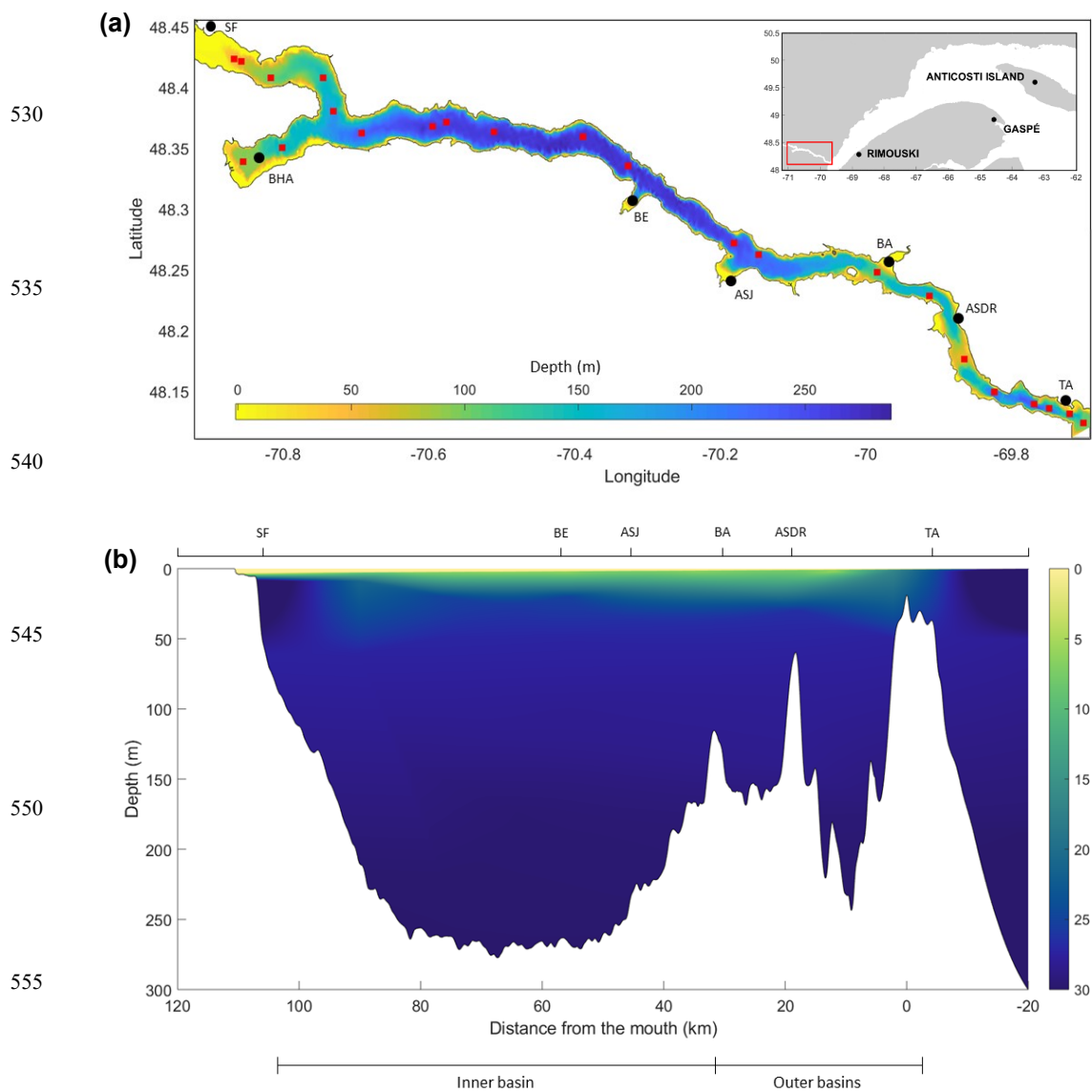
515

520

525

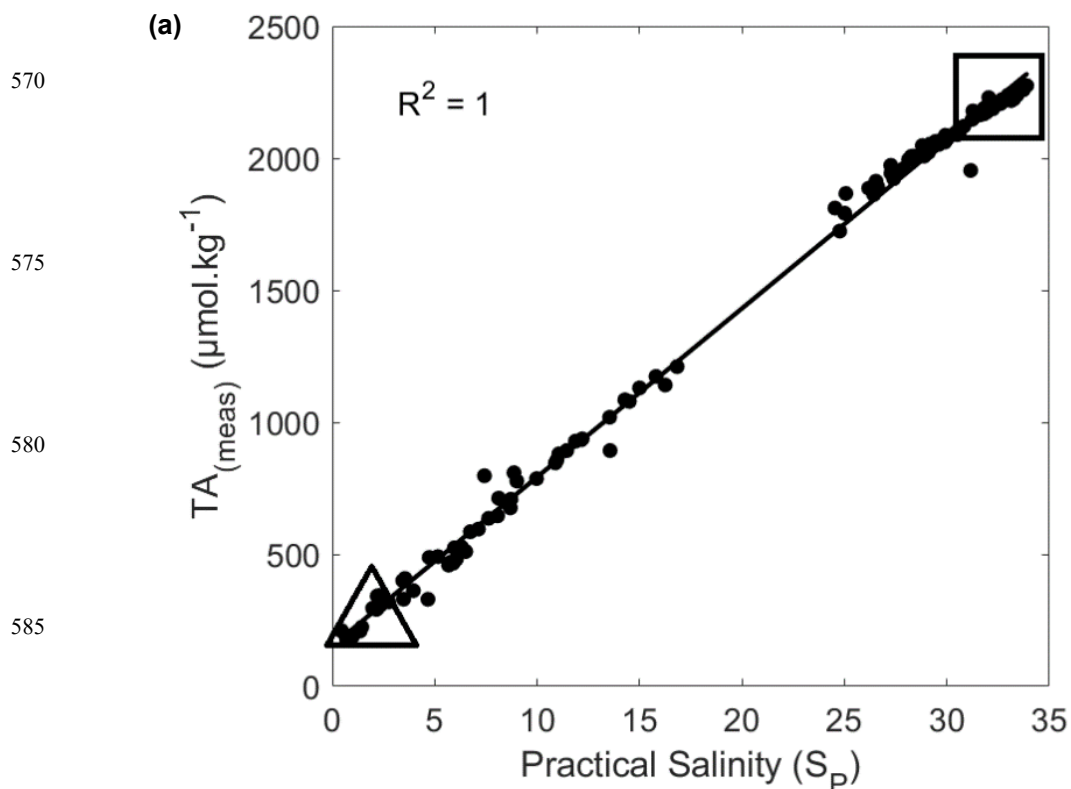


Figures



560 **Figure 1. a) Bathymetry and geographic location of the Saguenay Fjord. Red dots represent the hydrographic stations**
561 **sampled during R/V Coriolis II cruises. b) Longitudinal section of the Saguenay Fjord, showing the strong halocline. The**
562 **approximate location of the following are shown: Tadoussac (TA), L'Anse de Roche (ASDR), Baie Sainte-Marguerite**
563 **(BA), Anse-Saint-Jean (ASJ), Baie-Eternité (BE), St. Fulgence (SF), Baie des Ha! Ha! (BHA).**

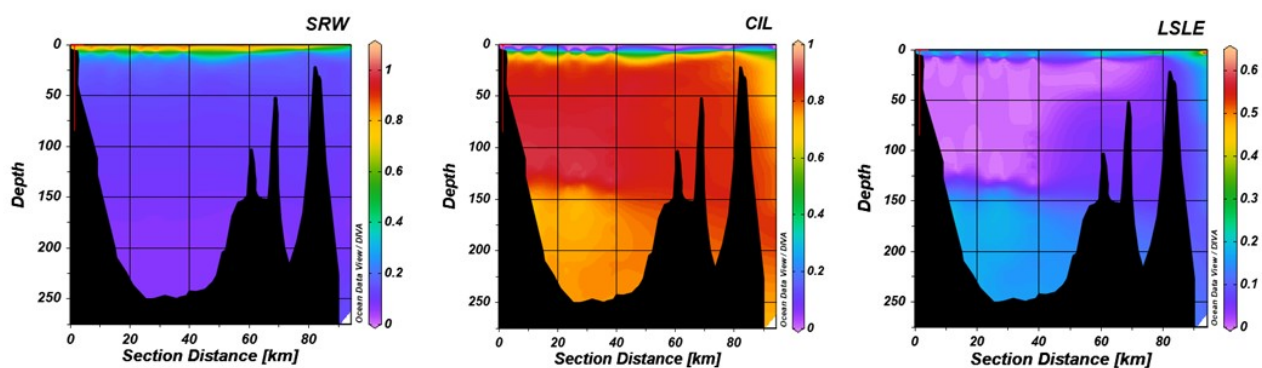
565



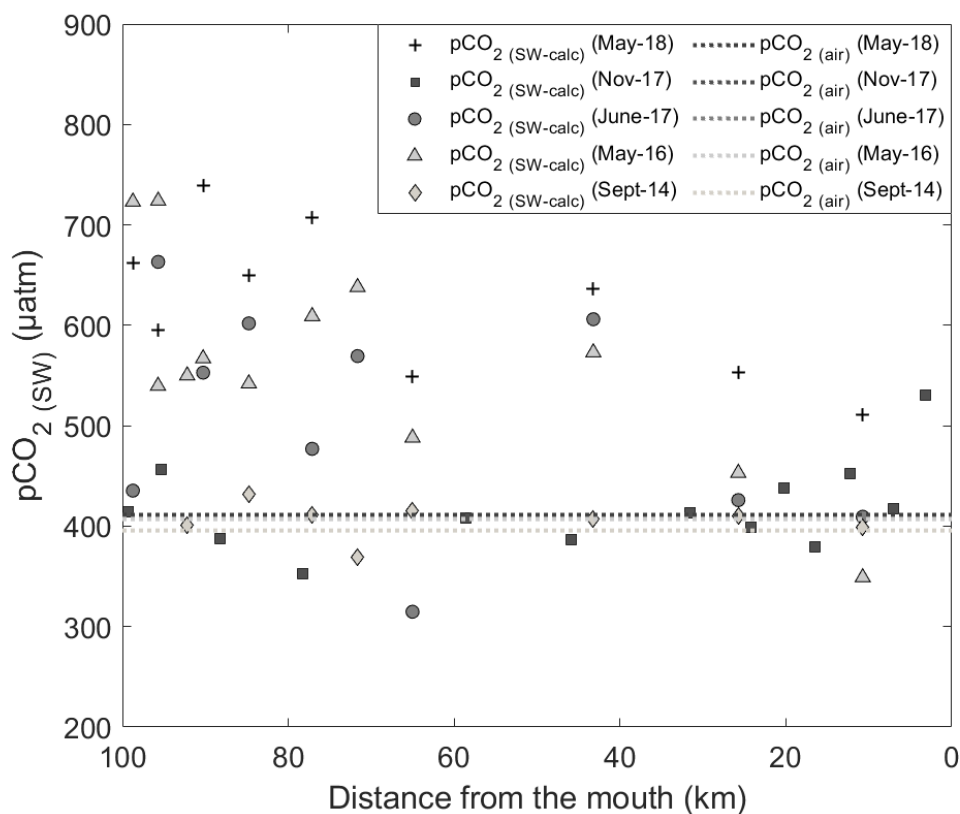
(b)

Saguenay River properties	
Practical salinity (S_P)	0.00 ± 0
$TA_{(meas)}$ ($\mu\text{mol}\cdot\text{kg}^{-1}$)	154 ± 52
$TA_{(calc)}$ ($\mu\text{mol}\cdot\text{kg}^{-1}$)	198 ± 51
Org Alk ($\mu\text{mol}\cdot\text{kg}^{-1}$)	-33 ± 3

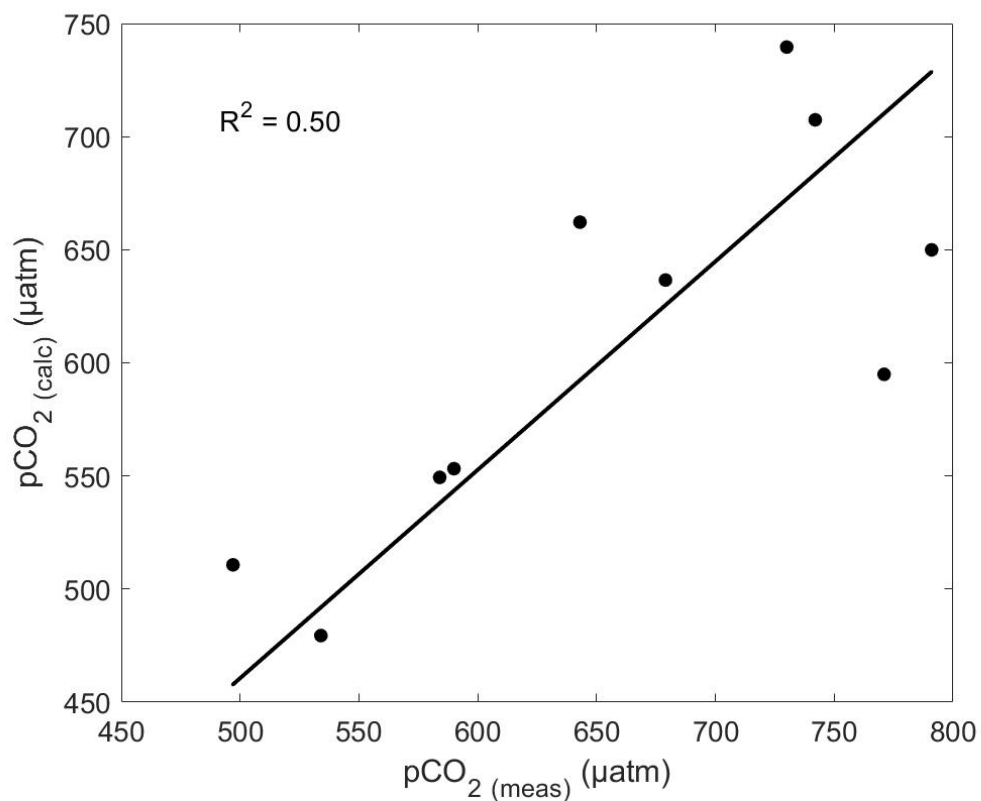
600 Figure 2. a) Measured alkalinity ($TA_{(meas)}$) versus practical salinity (S_P) for SRW and CIL data points, for all sampling months ($R^2 = 1$). The triangle defines the properties of the SRW, and the square comprises the properties of the CIL. b) $TA_{(meas)}$, $TA_{(calc)}$ and Org Alk definitions for the Saguenay River (SRW), using surface-water data from all sampling months, with standard error. The Org Alk (positive) contribution to the TA of the CIL is not considered as it accounts for less than 0.1 % of its TA.



605 **Figure 3.** Vertical sections showing the relative contributions of the Saguenay River (SRW), the St. Lawrence Estuary Cold Intermediate Layer (CIL) and Lower St. Lawrence Estuary bottom waters (LSLE) to the water column structure of the Saguenay Fjord (June 2017). Fractions were estimated using an Optimum Multi-Parameter (OMP) algorithm (Tomczak and Large, 1989; Tomczak, 1981; Mackas and Harrison, 1997). A Variational Analysis (DIVA) interpolation was applied between field data points in Ocean Data View.



610 **Figure 4. Spatial distribution of surface-water $pCO_{2(SW-calc)}$ in June 2017, November 2017, May 2016, September 2014 and May 2018. Dashed lines represent the $pCO_{2(air)}$ on the sampling months (respectively 396 ppm in September 2014, 407 ppm in May 2016, 408 ppm in June and November 2017, and 411 ppm in May 2018). Data points above the red line indicate that waters are sources of CO_2 to the atmosphere, whereas those below the red line identify waters that are sinks of atmospheric CO_2 .**



615 **Figure 5. Correlation between $p\text{CO}_2(\text{SW-meas})$ and $p\text{CO}_2(\text{SW-calc})$ for May 2018. The black line shows the linear regression with a null intercept ($R^2 = 0.50$).**

620

625

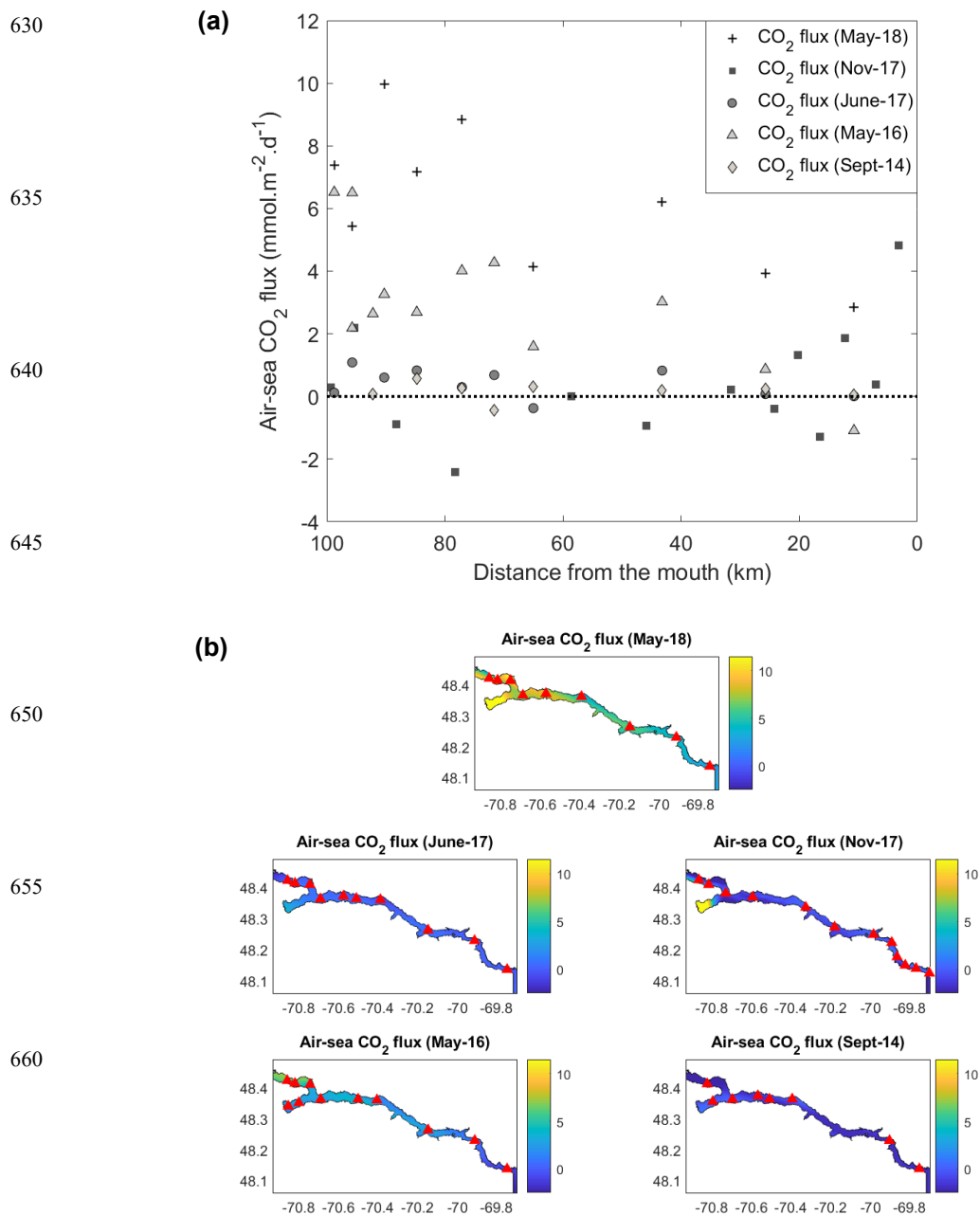


Figure 6. a) Spatial distribution of air-sea CO₂ flux (mmol·m⁻²·d⁻¹) in the Saguenay Fjord for all cruises. Data points above the red line indicate sources of CO₂ to the atmosphere, whereas those below the red line are sinks of atmospheric CO₂; b) Spatial interpolation of air-sea CO₂ fluxes (mmol·m⁻²·d⁻¹) in the Saguenay Fjord for all cruises. Red triangles indicate sampling locations.

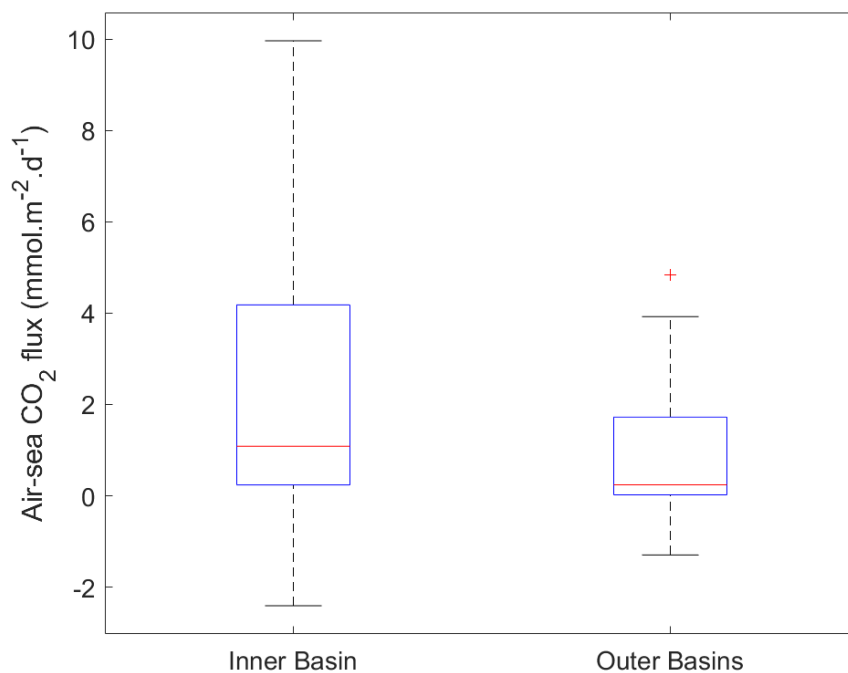
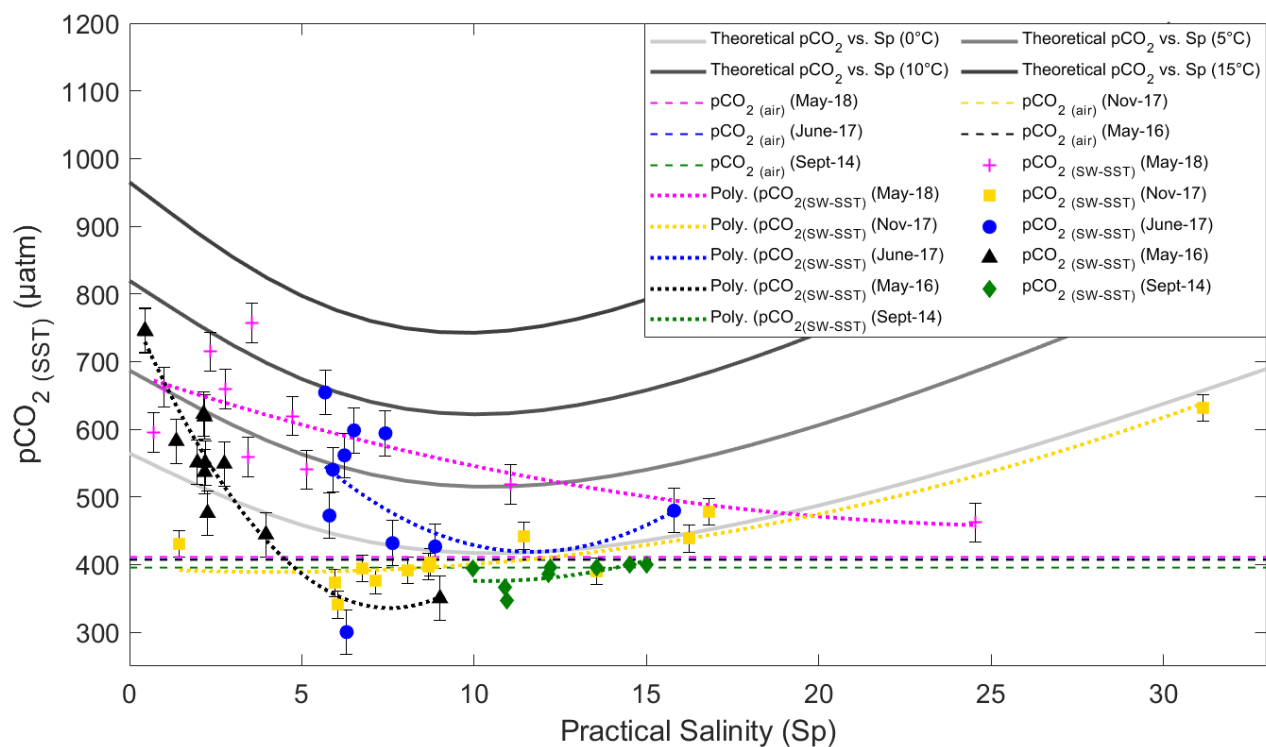
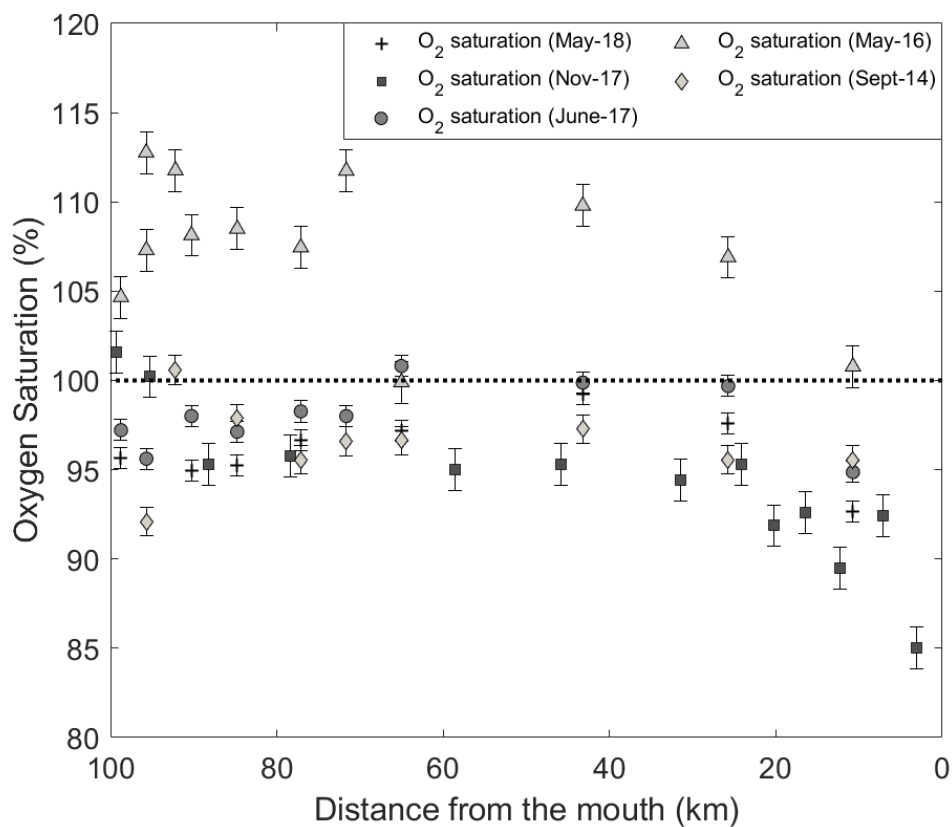


Figure 7. Box-plot of the air-sea CO₂ fluxes from all data in the two subsections of the study area (Inner basin and Outer basins). The red line is the median, the box spans the interquartile range (25-75 percentiles) and the whiskers show the extreme data points not considered outliers. One outlier is identified by the red + symbol.



674

675 **Figure 8.** Temperature-normalized field $pCO_{2(SW-SST)}$, and results of the conservative, two end-member mixing model for $pCO_{2(SW-SST)}$ in the Saguenay Fjord surface
 676 waters. Dashed lines represent the $pCO_{2(air)}$ on the sampling months (396 ppm in September 2014, 407 ppm in May 2016, 408 ppm in June and November 2017, and 411
 677 ppm in May 2018). Error bars show standard error of the mean for $pCO_{2(SW-SST)}$ values – bars are smaller than the symbol for September 2014.



678 Figure 9. Spatial distribution of surface-water dissolved O₂ saturation (%) in May 2018, June 2017, November 2017, May
679 2016 and September 2014. The dashed line represents equilibrium with the atmosphere (i.e., 100% saturation). Data
680 points above the line indicate that waters are supersaturated in O₂, whereas those below the line identify O₂-
681 undersaturated waters with respect to the atmosphere. Error bars show standard error of the mean for O₂ saturation
682 values.

683
684
685
686
687
688
689
690
691
692
693
694



695
696
697
698
699
700
701
702
703
704
705
706
707
708
709
710
711
712
713
714
715
716
717
718
719
720
721
722
723
724
725
726
727
728
729
730
731
732
733
734
735

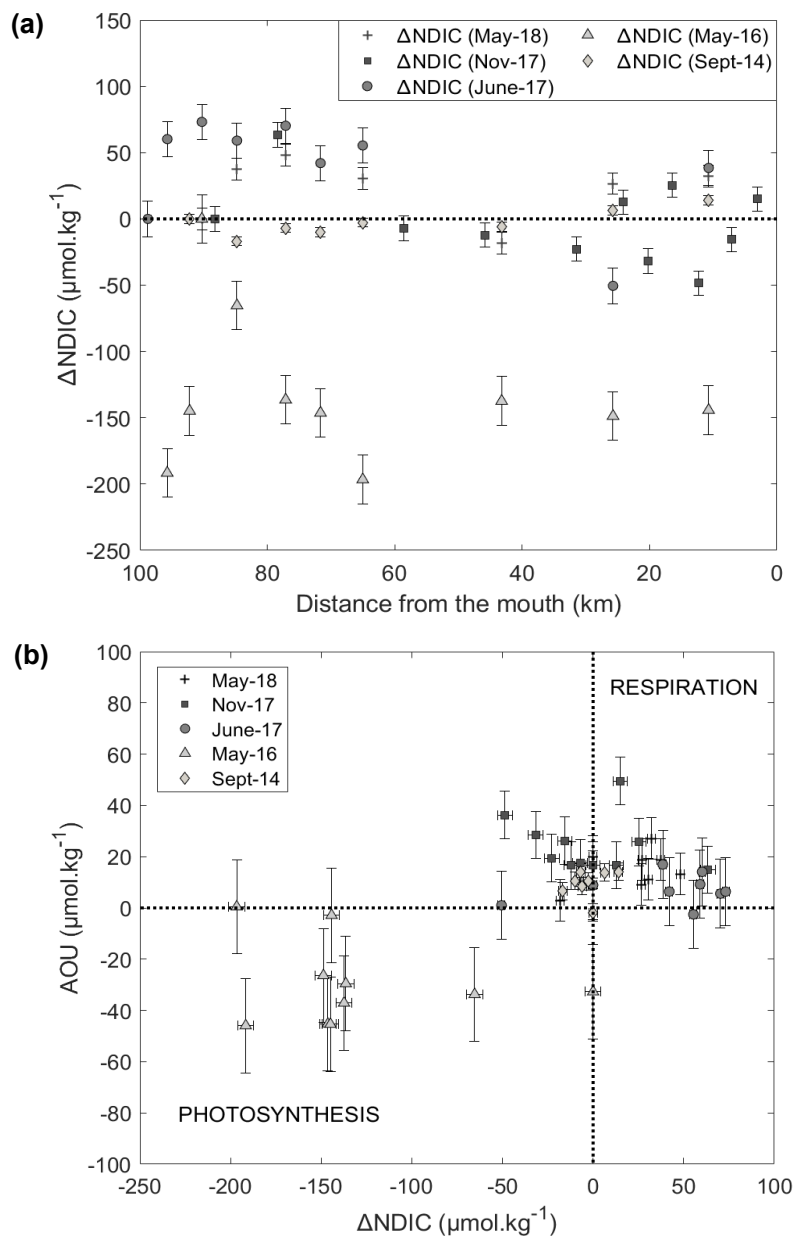


Figure 10. a) ΔNDIC (i.e. change in NDIC relative to the saline waters at the head of the fjord) distribution in the Saguenay Fjord surface waters. Data were normalized to a common salinity (average for each sampling period) according to the method of Friis *et al.* (2003); Error bars show standard error of the mean for NDIC values. b) Apparent oxygen utilization (AOU) against ΔNDIC . Error bars show standard error of the mean for AOU values.



736 Tables

737

SWT	Salinity	Temperature (°C)	TA _(meas) ($\mu\text{mol}\cdot\text{kg}^{-1}$)	$\delta^{18}\text{O}$ (per mil)	DIC ($\mu\text{mol}\cdot\text{kg}^{-1}$)	DO ($\mu\text{mol}\cdot\text{L}^{-1}$)
SRW	0.00 ± 0	6.19 ± 0.18	154 ± 13	-12.17 ± 0.21	230 ± 12	411 ± 6
CIL	32.52 ± 0.05	1.44 ± 0.08	2210 ± 2	-1.12 ± 0.03	2141 ± 3	256 ± 5
LSLE	34.31 ± 0.01	5.16 ± 0.18	2294 ± 2	-0.17 ± 0.02	2276 ± 3	76 ± 1
SLRW	0.00 ± 0	12.11 ± 0.13	1099 ± 16	-8.09 ± 0.13	1140 ± 15	329 ± 5
Weights	25	1	25	25	15	1

738

739 Table 1. Source-Water Type (SWT) definitions for the Saguenay River (SWR), the St. Lawrence Estuary summertime
 740 Cold Intermediate Layer (CIL), the Lower St. Lawrence Estuary bottom water (LSLE) and the St. Lawrence River
 741 (SLRW). Definitions and variances were derived from data taken in September 2014, May 2016, June 2017 and
 742 November 2017. Data for SRW and SLRW were extrapolated to $S_p = 0$. The weights used in the OMP analysis are also
 743 shown.

744

Sampling Month	pCO _{2(SW-calc)} (μatm)	k (cm h^{-1})	u (m s^{-1})	F ($\text{mmol}\cdot\text{m}^{-2}\cdot\text{d}^{-1}$)
May 2018	623 ± 26 (511/740)	1.94 ± 0.01 (1.89/1.97)	3.91	6.2 ± 0.79 (2.9/10.0)
November 2017	418 ± 12 (353/530)	3.2 ± 0.04 (2.82/3.38)	4.2	0.40 ± 0.51 (-2.4/4.8)
June 2017	506 ± 35 (315/663)	0.37 ± 0.01 (0.36/0.42)	1.89	0.42 ± 0.15 (-0.4/1.1)
May 2016	563 ± 31 (349/724)	1.26 ± 0.01 (1.15/1.30)	3.17	3.04 ± 0.62 (-1.1/6.5)
September 2014	406 ± 6 (369/432)	1.43 ± 0.01 (1.39/1.49)	3.71	0.16 ± 0.10 (-0.43/0.56)

745

746 Table 2. Mean, standard error of the mean and range of pCO_{2(SW)}, k, u and F in the Saguenay Fjord surface waters.
 747 Numbers in parentheses indicate the observed or calculated ranges. Overall, the total area-averaged degassing flux of the
 748 fjord adds up to $2.14 \pm 0.43 \text{ mmol}\cdot\text{m}^{-2}\cdot\text{d}^{-1}$ (i.e. $0.78 \pm 0.16 \text{ mol}\cdot\text{m}^{-2}\cdot\text{yr}^{-1}$).



Data availability

750 Data presented in this paper are available upon request from one of the authors (louise.delaigne@mail.mcgill.ca).



Appendix

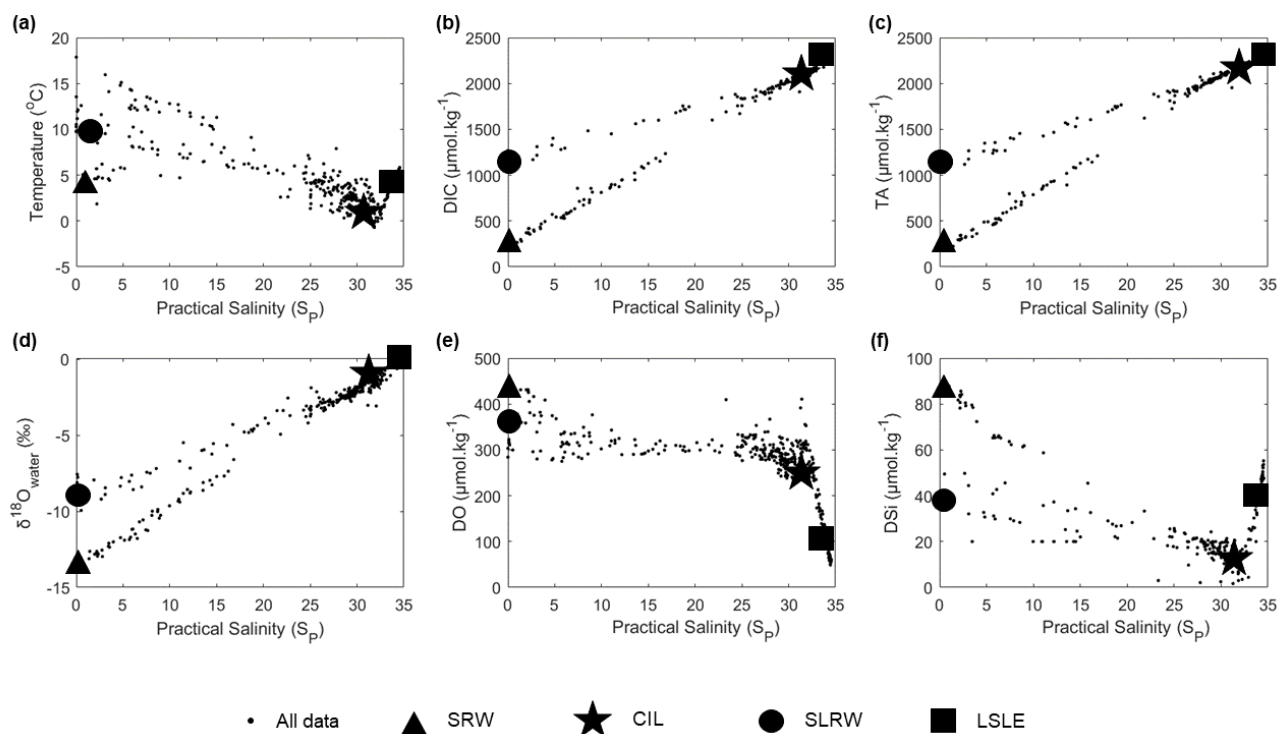


Figure A. a) Temperature, b) Dissolved Inorganic Carbon (DIC), c) Total Alkalinity (TA), d) $\delta^{18}\text{O}_{\text{water}}$, e) Dissolved Oxygen (DO), and f) Dissolved silicate (DSi) versus practical salinity (SP) for data from September 2014, May 2016, June 2017, November 2017 and May 2018. Each large symbol (square, circle, triangle and star) represents distinct source water masses.



Author contribution

A.M. and L.D. conceived the project. A.M. acquired and processed the data prior to 2016. L.D. conducted the data analysis
495 and wrote the first draft of the paper whereas A.M. provided editorial and scientific recommendations. H.T. provided results
of alkalinity and dissolved inorganic carbon analyses and scientific recommendations.

Competing interests

The authors declare that they have no conflict of interest.

Acknowledgements

500 We would like to give special thanks to Gilles Desmeules as well as the Captains and crew of the R/V Coriolis II
without whom, over the years, this project would not have been possible. Most of the data presented in this study were
acquired opportunistically on research cruises funded by Ship-Time Program grants to A.M. or Canadian colleagues by the
Natural Sciences and Engineering Research Council of Canada (NSERC). The work was funded by a Regroupement
Stratégique grant from the Fonds Québécois de Recherche Nature et Technologies (FQRNT) to GEOTOP as well as NSERC
505 Discovery and Marine Environmental Observation, Prediction and Response Network (MEOPAR; Canadian Ocean
Acidification Research partnership) grants to A.M and H.T. We would like to thank Dr. Jean-Francois Hélie at GEOTOP-
UQAM for carrying out the $\delta^{18}\text{O}_{\text{water}}$ analyses as well as Constance Guignard for cruise preparation and support in the
laboratory. Finally, L.D. wishes to thank MEOPAR and the Department of Earth and Planetary Sciences at McGill for
financial support in the form of stipends, scholarships and assistantships. Bathymetric data of the fjord were graciously
510 provided by Mélanie Belzile. Figure (3) in this study was created with the Ocean Data View Software (Schlitzer, 2015).

References

- Annane, S., St-Amand, L., Starr, M., Pelletier, E., and Ferreyra, G. A.: Contribution of transparent exopolymeric particles
(TEP) to estuarine particulate organic carbon pool, *Mar. Ecol. Prog. Ser.*, 529, 17-34, 2015.
- 515 Bauer, J. E., Cai, W. J., Raymond, P. A., Bianchi, T. S., Hopkinson, C. S., and Regnier, P. A.: The changing carbon cycle of
the coastal ocean, *Nature*, 504, 61-70, 2013.
- Bélangier, C.: Observation and modelling of a renewal event in the Saguenay Fjord, Ph.D thesis, Université du Québec à
Rimouski, Que., Canada, 2003.



520

Bellis, A.: Spectrophotometric determination of pH in estuarine waters using Phenol Red, B. Sc. thesis, McGill University, Montreal, Que., Canada, 53 pp., 2002.

525 Belzile, M., Galbraith, P. S., and Bourgault, D.: Water renewals in the Saguenay Fjord, *J. Geophys. Res-Oceans*, 121, 638-657, 2016.

Bourgault, D., Galbraith, P. S., and Winkler, G.: Exploratory observations of winter oceanographic conditions in the Saguenay Fjord, *Atmos. -Ocean*, 50, 17-30, 2012.

530 Brewer, P. G., and Peltzer, E. T.: Limits to marine life, *Science*, 324, 347-348, 2009.

Cai, W. J., and Wang, Y.: The chemistry, fluxes, and sources of carbon dioxide in the estuarine waters of the Satilla and Altamaha Rivers, Georgia, *Limnol. Oceanogr.*, 43, 657-668, 1998.

535 Cai, W. J., Wang, Y., and Hodson, R. E.: Acid-base properties of dissolved organic matter in the estuarine waters of Georgia, USA, *Geochim Cosmochim. Acta*, 62, 473-483, 1998.

Caldeira, K., and Wickett, M. E.: Ocean model predictions of chemistry changes from carbon dioxide emissions to the atmosphere and ocean, *J. Geophys. Res-Oceans*, 110, 2005.

540

Chassé, R., and Côté, R.: Aspects of winter primary production in the upstream section of Saguenay Fjord, *Hydrobiologia*, 215, 251-260, 1991.

Chester, R. (Eds.): *Marine Geochemistry*, Springer, Netherlands, 702 pp., 1990.

545

Clayton, T. D., and Byrne, R. H.: Spectrophotometric seawater pH measurements: total hydrogen ion concentration scale calibration of m-cresol purple and at-sea results, *Deep-Sea Res. Pt. I*, 40, 2115-2129, 1993.

550 Dickie, L. M. and Trites, R. W.: The Gulf of St. Lawrence, in: *Estuaries and Enclosed Seas, Ecosystems of the World 26*, edited by: Ketchum, B. H., Elsevier, 403-425, 1983.

Dickson, A. G., Sabine, C. L., and Christian, J. R.: *Guide to Best Practices for Ocean CO₂ Measurements*, PICES Special Publication 3, 191 pp., Sidney, BC, Canada, 2007.



555 Dinauer, A., and Mucci, A.: Spatial variability in surface-water pCO₂ and gas exchange in the world's largest semi-enclosed estuarine system: St. Lawrence Estuary (Canada), *Biogeosciences*, 14, 3221-3237, 2017.

Dinauer, A., and Mucci, A.: Distinguishing between physical and biological controls on the spatial variability of pCO₂: A novel approach using OMP water mass analysis (St. Lawrence, Canada), *Mar. Chem.*, 204, 107-120, 2018.

560

Doney, S. C., Fabry, V. J., Feely, R. A., and Kleypas, J. A.: Ocean acidification: The Other CO₂ Problem, *Ann. Rev. Mar. Sci.*, 1, 169–192, 2009.

565 Douglas, N. K., and Byrne, R. H.: Achieving accurate spectrophotometric pH measurements using unpurified meta-cresol purple, *Mar. Chem.*, 190, 66-72, 2017.

El-Sabh, M. I., and Silverberg, N.: The St. Lawrence Estuary: Introduction, in: *Oceanography of a Large-Scale Estuarine System*, edited by: El-Sabh, M. I. and Silverberg, N., Springer-Verlag, New York, NY, 1-9, 1990.

570 Epstein, S., and Mayeda, T.: Variation of O¹⁸ content of waters from natural sources, *Geochim. Cosmochim. Acta*, 4, 213-224, 1953.

Friis, K., Körtzinger, A., and Wallace, D. W.: The salinity normalization of marine inorganic carbon chemistry data, *Geophys. Res. Lett.*, 30, 2003.

575

Galbraith, P. S.: Winter water masses in the Gulf of St. Lawrence, *J. Geophys. Res-Oceans*, 111, C06022, 2006.

Gilbert, D., and Pettigrew, B.: Interannual variability (1948-1994) of the CIL core temperature in the Gulf of St. Lawrence, *Can. J. Fish. Aquat. Sci.*, 54, 57-67, 1997.

580

Grasshoff, K., Kremling, K., and Ehrhardt, M. (Eds.): *Methods of Seawater Analysis 3rd Edn.*, Wiley-VCH, Weinheim, Germany, 1999.

585 Gratton, Y., Mertz, G., and Gagné, J. A.: Satellite observations of tidal upwelling and mixing in the St. Lawrence Estuary, *J. Geophys. Res-Oceans*, 93, 6947-6954, 1988.



Hönisch, B., Ridgwell, A., Schmidt, D.N., Thomas, E., Gibbs, S.J., Sluijs, A., Zeebe, R., Kump, L., Martindale, R.C., Greene, S.E. and Kiessling, W.: The geological record of ocean acidification, *Science*, 335, 1058-1063, 2012.

590 Hunt, C. W., Snyder, L., Salisbury, J. E., Vandemark, D., and McDowell, W. H.: SIPCO₂: A simple, inexpensive surface water pCO₂ sensor, *Limnol. Oceanogr-Meth.*, 15, 291-301, 2017.

Jiang, L. Q., Cai, W. J., and Wang, Y.: A comparative study of carbon dioxide degassing in river-and marine dominated estuaries, *Limnol. Oceanogr.*, 53, 2603-2615, 2008.

595

Karstensen, J.: OMP (Optimum Multiparameter) analysis - USER GROUP. Retrieved from <http://omp.geomar.de/>, 2013.

Karstensen, J., and Tomczak, M.: Age determination of mixed water masses using CFC and oxygen data, *J. Geophys. Res-Oceans*, 103, 18599-18609, 1998.

600

Ko, Y. H., Lee, K., Eom, K. H., and Han, I. S.: Organic alkalinity produced by phytoplankton and its effect on the computation of ocean carbon parameters, *Limnol. Oceanogr.*, 61, 1462-1471, 2016.

Lansard, B., Mucci, A., Miller, L. A., Macdonald, R. W., and Gratton, Y.: Seasonal variability of water mass distribution in the southeastern Beaufort Sea determined by total alkalinity and $\delta^{18}\text{O}$, *J. Geophys. Res-Oceans*, 117, 2012.

605

Levasseur, M. E., and Therriault, J. C.: Phytoplankton biomass and nutrient dynamics in a tidally induced upwelling: the role of the NO₃: SiO₄ ratio, *Mar. Ecol. Prog. Ser.*, 39, 87-97, 1987.

610 Lueker, T. J., Dickson, A. G., and Keeling, C. D.: Ocean pCO₂ calculated from dissolved inorganic carbon, alkalinity, and equations for K₁ and K₂: validation based on laboratory measurements of CO₂ in gas and seawater at equilibrium, *Mar. Chem.*, 70, 105-119, 2000.

Lüthi, D., Le Floch, M., Bereiter, B., Blunier, T., Barnola, J.M., Siegenthaler, U., Raynaud, D., Jouzel, J., Fischer, H., Kawamura, K. and Stocker, T.F.: High-resolution carbon dioxide concentration record 650,000–800,000 years before present, *Nature*, 453, 2008.

615

Mackas, D. L., Denman, K. L., and Bennett, A. F.: Least squares multiple tracer analysis of water mass composition, *J. Geophys. Res-Oceans*, 92, 2907-2918, 1987.

620



Mackas, D. L., and Harrison, P. J.: Nitrogenous nutrient sources and sinks in the Juan de Fuca Strait/Strait of Georgia/Puget Sound estuarine system: assessing the potential for eutrophication, *Estuar. Coast Shelf Sci.*, 44, 1-21, 1997.

Millero, F. J.: The pH of estuarine waters, *Limnol. Oceanogr.*, 31, 839-847, 1986.

625

Mucci, A., Levasseur, M., Gratton, Y., Martias, C., Scarratt, M., Gilbert, D., Tremblay, J.É., Ferreyra, G. and Lansard, B.: Tidally induced variations of pH at the head of the Laurentian Channel, *Can. J. Fish. Aquat. Sci.*, 75, 1128-1141, 2017.

Mucci, A., Starr, M., Gilbert, D., and Sundby, B.: Acidification of lower St. Lawrence Estuary bottom waters, *Atmos.-Ocean*, 49, 206-218, 2011.

Orr, J. C.: Recent and future changes in ocean carbonate chemistry, in: *Ocean acidification*, edited by: Gattuso, J.-P. and Hansson, L., Oxford University Press, Oxford, UK, 1, 25 pp., 2011.

Pierrot, D., Lewis, E., and Wallace, D. W. R.: MS Excel Program Developed for CO₂ System Calculations, ORNL/CDIAC-105a, Carbon Dioxide Information Analysis Center, Oak Ridge National Laboratory, U.S. Department of Energy, Oak Ridge, Tennessee, 2006.

Piper, D. J. W., Mudie, P. J., Fader, G. B., Josenhans, H. W., MacLean, B., and Vilks, G.: Quaternary Geology, Chapter 10, in: *Geology of the Continental Margin of Eastern Canada (Vol. 2)*, Geological Survey of Canada, edited by: Keen, M. J. and William, G. L., Canada, 1990.

Rhein, M., Rintoul, S.R., Aoki, S., Campos, E., Chambers, D., Feely, R.A., Gulev, S., Johnson, G.C., Josey, S.A., Kostianoy, A., Mauritzen, C., Roemmich, D., Talley, L.D., and Wang, F.: Observations: Ocean, in: *Climate Change 2013: The Physical Science Basis*, Contribution of Working Group I to the Fifth Assessment Report of the Intergovernmental Panel on Climate Change, edited by: Stocker, T.F., Qin, D., Plattner, G.-K., Tignor, M., Allen, S.K., Boschung, J., Nauels, A., Xia, Y., Bex, V. and Midgley, P.M., Cambridge University Press, Cambridge, United Kingdom and New York, NY, USA, 2013.

Robert-Baldo, G. L., Morris, M. J., and Byrne, R. H.: Spectrophotometric determination of seawater pH using phenol red, *Anal. Chem.*, 57, 2564-2567, 1985.

650

Saucier, F. J., and Chassé, J.: Tidal circulation and buoyancy effects in the St. Lawrence Estuary, *Atmos.Ocean*, 38, 505-556, 2000.



Smith, J. N., and Walton, A.: Sediment accumulation rates and geochronologies measured in the Saguenay Fjord using the
655 Pb-210 dating method, *Geochim. Cosmochim. Acta*, 44, 225-240, 1980.

Stacey, M. W., and Gratton, Y.: The energetics and tidally induced reverse renewal in a two-silled fjord, *J.Phys. Oceanogr.*,
31, 1599-1615, 2001.

660 Telmer, K., and Veizer, J.: Carbon fluxes, pCO₂ and substrate weathering in a large northern river basin, Canada: carbon
isotope perspectives, *Chem. Geol.*, 159, 61-86, 1999.

Therriault, J. C., and Lacroix, G.: Penetration of the deep layer of the Saguenay Fjord by surface waters of the St. Lawrence
Estuary, *Journal of the Fisheries Board of Canada*, 32, 2373-2377, 1975.

665

Tomczak Jr, M.: An analysis of mixing in the frontal zone of South and North Atlantic Central Water off North-West Africa,
Prog. Oceanogr., 10, 173-192, 1981.

Tomczak, M.: Potential vorticity as a tracer in quantitative water mass analysis, *International WOCE Newsletter*, 36, 6-10,
670 1999.

Tomczak, M., and Large, D. G.: Optimum multiparameter analysis of mixing in the thermocline of the eastern Indian Ocean,
J. Geophys. Res-Oceans, 94, 16141-16149, 1989.

675 Tremblay, L., and Gagné, J. P.: Organic matter distribution and reactivity in the waters of a large estuarine system, *Mar.*
Chem., 116, 1-12, 2009.

Wanninkhof, R.: Relationship between wind speed and gas exchange over the ocean revisited, *Limnol. Oceanogr.-Meth.*, 12,
351-362, 2014.

680

Wanninkhof, R.: Relationship between wind speed and gas exchange over the ocean, *J. Geophys. Res Oceans*, 97, 7373-
7382, 1992.

Weiss, R.: Carbon dioxide in water and seawater: the solubility of a non-ideal gas, *Mar. Chem.*, 2, 203-215, 1974.

685

Weiss, R. F., and Price, B. A.: Nitrous oxide solubility in water and seawater, *Mar. Chem.*, 8, 347-359, 1980.



Xie, H., Aubry, C., Bélanger, S., and Song, G.: The dynamics of absorption coefficients of CDOM and particles in the St. Lawrence estuarine system: Biogeochemical and physical implications, *Mar. Chem.*, 128, 44-56, 2012.

690

Zakardjian, B. A., Gratton, Y., and Vézina, A. F.: Late spring phytoplankton bloom in the Lower St. Lawrence Estuary: the flushing hypothesis revisited, *Mar. Ecol. Prog. Ser.*, 192, 31-48, 2000.

Zeebe, R. E., and Wolf-Gladrow, D. (Eds.): *CO₂ in seawater: equilibrium, kinetics, isotopes*, Elsevier Oceanography Series 65, Amsterdam, 2001.